A Journal of the Gesellschaft Deutscher Chemiker

Angewandte International Edition GDCh Chemie

www.angewandte.org

Accepted Article

Title: Coulombic Condensation of Liquefied Gas Electrolytes for Li Metal Batteries at Ambient Pressure

Authors: Yijie Yin, John Holoubek, Kangwoon Kim, Alex Liu, Bhargav Bhamwala, Shen Wang, Bingyu Lu, Kunpeng Yu, Hongpeng Gao, Mingqian Li, Ganesh Raghavendran, Guorui Cai, Weikang Li, Ping Liu, Ying Shirley Meng, and Zheng Chen

To be cited as: *Angew. Chem. Int. Ed.* **2024**, e202420411

Link to VoR: https://doi.org/10.1002/anie.202420411

WILEY VCH

10.1002/anie.202420411

Coulombic Condensation of Liquefied Gas Electrolytes for Li Metal Batteries at Ambient Pressure

Yijie Yin[1,†], John Holoubek[2,†], Kangwoon Kim[2], Alex Liu [2], Bhargav Bhamwala [2], Shen Wang[2], Bingyu Lu[2], Kunpeng Yu[2], Hongpeng Gao[2], Mingqian Li[2], Ganesh Raghavendran[2], Guorui Cai[2], Weikang Li[2], Ping Liu[1,2,3,], Ying Shirley Meng[2,3,4], Zheng Chen[1,2,3*]*

[1]Program of Materials Science and Engineering, University of California, San Diego, La Jolla, CA 92093, USA

[2]Aiiso Yufeng Li Family Department of Chemical and Nano Engineering, University of California, San Diego, La Jolla, CA 92093, USA

[3]Sustainable Power and Energy Center, University of California, San Diego, La Jolla, CA 92093, USA

[4]Pritzker School of Molecular Engineering, University of Chicago, Chicago, IL 60637, USA

[†]These authors contributed equally to this work.

**Correspondence to: zhengchen@eng.ucsd.edu, shirleymeng@uchicago.edu*

10.1002/anie.202420411

Abstract:

The concept of employing highly concentrated electrolytes has been widely incorporated into electrolyte design, due to their enhanced Li-metal passivation and oxidative stability compared to their diluted counterparts. However, issues such as high viscosity and sub-optimal wettability, compromise their suitability for commercialization. In this study, we present a highly concentrated dimethyl ether-based electrolyte that appears as a liquid phase at ambient conditions via Li^+ - solvents ion-dipole interactions (Coulombic condensation). Unlike conventional high salt concentration ether-based electrolytes, it demonstrates enhanced transport properties and fluidity. The anion-rich solvation structure also contributes to the formation of a LiF-rich salt-derived solid electrolyte interphase, facilitating stable Li metal cycling for over 1000 cycles at 0.5 mA cm^{-2}, 1 mAh cm^{-2} condition. When combined with a sulfurized polyacrylonitrile (SPAN) electrode, the electrolyte effectively reduces the polysulfide shuttling effect and ensures stable performance across a range of charging currents, up to 6 mA cm^{-2}. This research underscores a promising strategy for developing an anion-rich, high concentration ether electrolyte with decreased viscosity, which supports a Li metal anode with exceptional temperature durability and rapid charging capabilities.

Introduction

As the transportation sector rapidly electrifies, the demand for high performance energy storage systems working over a wide temperature range is significantly stimulated. However, as the conventional Li-ion chemistry is reaching its performance limit, new chemistries must be implemented for continuous progress. Li metal, with its superior specific capacity (3860 mAh g^{-1}), low reduction potential (−3.04 V vs. standard hydrogen electrode), and minimal solid density (0.534 g cm^{-3}), stands as the prime candidate for advanced high-energy density batteries[1]. Yet, practical application is hindered by the poor cyclability and safety concerns, stemming from the formation of dendritic and "dead" lithium by continuous parasitic reactions with electrolytes over cycling[2].

In conjunction with the Li metal anode, sulfurized polyacrylonitrile (SPAN) is identified as a promising cathode material. SPAN features short-chain sulfur covalently bonded to a conductive pyridine polymer matrix[3],[4]. This structure allows for the reversible cleavage and reformation of S-S chains during lithiation and de-lithiation processes[5]. Compared to alternative cathode materials, such as elemental sulfur and transition metal cathodes, SPAN cathodes offer (1) cost-effectiveness due to their metal-free composition; (2) improved kinetics, facilitated by the conductive polymer matrix to which the sulfur is bonded; and (3) superior cycling stability, attributed to a 'shuttle-free' short chain sulfur reaction mechanism. Presently, Li-SPAN batteries achieve high specific capacities of over 700 mAh g^{-1} and demonstrate cycling stability exceeding 1000 cycles[6],[7],[8].

Although Li metal and SPAN show promise as an excellent anode-cathode pair, there exists a mismatch in electrolyte compatibility between these two materials. Conventional carbonate

electrolytes, while compatible with SPAN cathodes, fail to adequately stabilize Li metal anodes. This inadequacy manifests as diminished Coulombic efficiency (CE) and dendritic lithium growth, both of which significantly curtail the battery's cycle life. Conversely, ether-based electrolytes improve the CE of Li metal anodes, but facilitate polysulfide dissolution from the SPAN polymer matrix, adversely affecting the stability of the cathode[9],[10]. With the adoption of low concentration weakly coordinated diethyl ether (DEE) and dibutyl ether (DBE) electrolytes[11-12], polysulfide dissolution issues can be mitigated in SPAN, but the fast-charging evaluation for Li/SPAN has not yet been explored.

Another option for rendering the electrolyte mismatch between Li metal anode and SPAN cathode, is to apply highly concentrated electrolyte (HCE). Benefitting from the significant decrease of free solvent, the HCE can reduce polysulfide dissolution by generating the salt-derived cathode/electrolyte interface (CEI) on SPAN side[13]. As for the Li metal side, high bulk ion concentration in the HCE reduces the concentration gradient at the solid/electrolyte interface (SEI) and maximizing Sand's time[14]. Therefore, the Li dendrite growth is limited. However, HCE suffers from the reduced ionic conductivity owing to high viscosity, along with low ionicity from ion-pairing, raising issues for fast charging and low-temperature operation. The increased viscosity of the HCE might also impact the wettability of separators and electrodes, further complicating the cell formation process[6]. Using non-coordinating diluents and ethers, localized highly concentrated electrolytes (LHCE) can reduce lithium salt concentration and viscosity, maintaining a Li^+ solvation structure similar to that in HCE[15]. However, LHCE struggles with achieving optimal ionic conductivity due to strong ion-pairing, affecting fast-charging[16]. Additionally, the selection of fluorinated diluent molecules in LHCE is crucial for interfacial chemistry, affecting Li^+ diffusion and cell impedance growth over time[17]. HCEs and LHCEs frequently fail to meet

the stringent requirements for battery performance in non-constant temperature environments, particularly under extreme weather conditions. The precipitation of salts from HCE and LHCE at subzero temperatures, coupled with the volatilization of ether-based electrolytes at elevated temperatures, presents significant safety concerns and leads to early battery failure[18],[19-20].

In this work, we introduce a strategy for HCE systems in batteries that are compatible with both Li and SPAN, in the meantime, ensuring a broad operational temperature window. The electrolyte with improved ion conductivity deploys an ultra-low viscosity solvent dimethyl ether (Me_2O) that is typically under gas phase with 593 kPa vapor pressure at 25 °C. Given that Me_2O has strong Li^+ solvating ability, it is hypothesized that the presence of lithium salts can significantly elevate the boiling point of Me_2O. This elevation is attributed to the stabilizing influence of ion-dipole interactions between the Li^+ ions and the Me_2O molecules. These interactions lead to a reduction in the volatility of the solvent, thereby increasing its boiling point. We refer to this phenomenon as 'Coulombic condensation'. Subsequently, we prove Me_2O can be condensed with lithium bis(fluorosulfonyl)imide (LiFSI) salt at ambient pressure experimentally. This LiFSI-Me_2O combination can form an ambient-pressure stable liquefied gas electrolyte. The saturated LiFSI concentration in Me_2O (Sat. LiFSI-Me_2O) remains stable from –60 to 60 °C and shows improved thermal stability compared with 4 M LiFSI in DME (4 M LiFSI-DME) which has a similar LiFSI: ether molar ratio of 1:2.4. Such electrolyte also offers comparative viscosity and ionic conductivity (> 5.5 mS cm^{-1}) at 20 °C, but much reduced viscosity and improved ionic conductivities at subzero temperatures compared with 4 M LiFSI-DME. In addition, benefiting from the good reductive stability of ethers and the formation of a salt-derived SEI, stable cycling of Li metal with 99.2% average CE over 1000 cycles can be achieved. When paired with SPAN electrode, the excess Li/SPAN cells demonstrate > 92% capacity retention over 200 cycles mostly

due to the reduced polysulfide dissolution and the formation of salt-derived SEI/CEIs. The cell using Sat. LiFSI-Me_2O electrolyte also withstands high charge current densities up to 6 mA cm^{-2} under a limited Li reservoir. This study shows that coulombic condensation in liquefied gas electrolytes enables a stable, high-conductivity ether-based solution, boosting lithium metal battery performance.

Results and Discussion

For designing the Coulombic Condensed electrolyte, Me_2O, which exists at gaseous state at standard temperature and pressure (STP) conditions (boiling point: –28 ºC at STP) is selected as the solvent. The material has been demonstrated to act as a promising liquefied gas solvent for enabling next-generation lithium-ion batteries due to its chemical and electrochemical Li metal compatibility[21-22]. Distinct from hydrofluorocarbons, Me_2O exhibits improved solubility of LiFSI salt in liquefied gas solvents due to the more polar ether functional group. Although Me_2O exhibits a boiling point far beneath room temperature, we hypothesize that this value could be substantially elevated in the presence of salt with sufficient ion-dipole interactions upon dissolution. We select LiFSI as a salt to demonstrate this concept due to its excellent Li-metal compatibility and high solubility in ethers[23-25]. Although the 35 – 40 ºC boiling point elevation required to yield a stable room-temperature solution is significant, the empirically linear dependence of boiling point elevation on salt concentration suggests that high-concentration solutions of LiFSI and Me_2O may be stable. To test this hypothesis, LiFSI salt is first loaded into a high-pressure window cell, then filled with Me_2O gas, producing a transparent solution with a low concentration (around 1M) (**Fig. 1a**). The LiFSI salt concentration of the solution increases as the pressure of the system is decreased by slowly releasing Me_2O gas from the cell within 10 minutes. Once the gas is

10.1002/anie.202420411

completely released, we observe a stable liquid at atmospheric pressure with a measured salt: ether molar ratio of 1: 2.36 (**Supplementary Fig. 1 and 2**). This confirms that, at sufficiently high salt concentrations, the favorable solvation energy between LiFSI and Me_2O is sufficient to elevate the boiling point of the solution above room temperature. The proposed solvation structure contains significantly fewer free Me_2O molecules, instead featuring a considerable number of Li^+-FSI^--Me_2O aggregates, as illustrated in **Fig. 1b**.

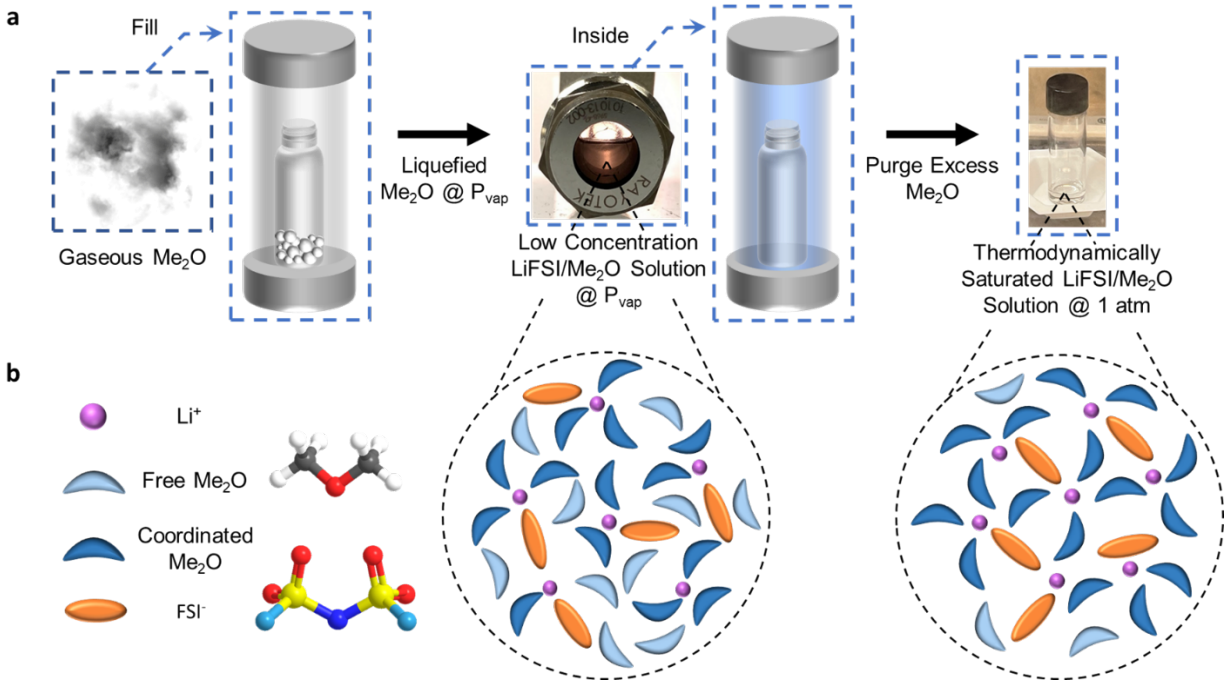

Figure 1. Design of the Condensed Electrolytes. (a) The workflow of obtaining thermodynamically Sat. LiFSI-Me_2O electrolytes at ambient pressure condition. (b) Proposed solvation structures for the low concentration LiFSI in Me_2O under its vapor pressure condition and the Sat. LiFSI-Me_2O at 1 atmosphere. Colors: Li^+, purple; C, dark grey; O, red; S, yellow; N, naval blue; F, cyan; H, white.

To testify the physical properties and electrochemical stability of the condensed electrolyte, a series of characterizations are performed for the pure DME solvent, 4 M LiFSI-DME, 11 M LiFSI in DME (~Sat. LiFSI-DME) and Sat. LiFSI-Me_2O. As shown in **Fig. 2a** and **Supplementary Fig.**

3, the differential scanning calorimetry (DSC) and the thermogravimetric analysis (TGA) reveal that pure DME is volatile, boiling at temperatures above 75°C. As LiFSI salt concentration increases, the boiling point is delayed to higher temperatures, exceeding 125°C for a 4 M salt concentration and surpassing 185°C at saturation. Whereas Sat. LiFSI-Me_2O does not show an obvious endothermic peak and the mass loss rate remains similar compared with 4 M LiFSI-DME before 172 ºC. When the temperature reaches > 210 ºC, LiFSI will decompose and generate a significant exothermic peak[26]. Based on **Fig. 2a**, we can observe that the exothermic peak of LiFSI decomposition is delayed for the Sat. LiFSI-Me_2O system, indicating its improved thermal stability. To understand the fluidity of different electrolytes at room temperature, the viscosity is measured and shown in **Fig. 2c** and **Supplementary Table 1**. The viscosity of pure DME, measured at approximately 0.42 mPa·s, aligns with literature reports[27]. As LiFSI concentration increases, viscosity significantly rises from 0.92 mPa·s at 1 M LiFSI-DME to 21.65 mPa·s and 140.29 mPa·s for 4 M LiFSI-DME and saturated LiFSI-DME, respectively, as expected. Notably, the viscosity of saturated LiFSI-Me_2O, at around 27.74 mPa·s, is slightly higher than that of 4 M LiFSI-DME, likely due to stronger Coulombic interactions at higher salt concentrations. The ionic conductivities of the 1 M $LiPF_6$ in EC:EMC (3:7 wt%), 1 M LiFSI-Me_2O, 4 M LiFSI-DME, Sat. LiFSI-Me_2O and Sat. LiFSI-DME electrolytes are shown in **Fig 2b and Supplementary Table 2**. It can be observed 1 M LiFSI-Me_2O retains a high ionic conductivity across the wide temperature range without noticeable drop, consistent with previous reports[21-22]. The ionic conductivities of Sat. LiFSI-Me_2O decline with the reduction of temperature although Sat. LiFSI-Me_2O electrolyte demonstrates a more modest decrease in conductivity with respect to reduced temperatures, maintaining comparable values compared to 1 M $LiPF_6$ in EC:EMC (3:7 wt%) at ultra-low temperatures. Regarding ionic conductivities of Sat. LiFSI-DME and 4 M LiFSI-DME, an obvious

turning point is observed around 0 ºC, indicating a phase change, substantiated by nonlinear Arrhenius behavior.

To further analyze the relationship between the solvation structure of LiFSI in Me_2O or DME electrolytes and study the LiFSI concentration impact on the solvation structure, Raman spectroscopy was utilized. The spectra, shown in **Fig. 2d**, **2e**, and **2f**, compare the effects of varying LiFSI concentrations in Me_2O and DME electrolytes against the baseline spectra of pure LiFSI salt and Me_2O solvent. In **Fig. 2d**, the characteristic S-N-S bending peak of the FSI^- at 774 cm^{-1} can be observed from the pure LiFSI which undergoes a significant red shift to 720 cm^{-1} in 1 M LiFSI-DME electrolyte. Furthermore, an upshift is observed for higher concentrations of LiFSI as seen in the 4 M and Sat. LiFSI-DME Raman spectra compare to 1 M LiFSI-DME, indicating an increase in the Li^+/FSI^- interactions, which is a characteristic of contact-ion pair (CIP) and aggregate (AGG) structures typically formed in high concentration electrolytes[11, 28]. Similarly, the characteristic FSI^- peak in LiFSI-Me_2O electrolyte shifts with varying LiFSI concentrations, showing a minor adjustment from 774 cm^{-1} to 725 cm^{-1} for 1 M LiFSI-Me_2O, compared to the shift from 774 cm^{-1} to 718 cm^{-1} for 1 M LiFSI-DME. This indicates Me_2O's weaker Li^+ solvation capacity, resulting in intensified cation-anion interactions within the LiFSI-Me_2O system at equivalent salt concentrations. At saturated states, the S-N-S bending peak at 775 cm^{-1} is shifted to 750 cm^{-1} in both the LiFSI-Me_2O and LiFSI-DME electrolytes which signifies comparable degrees of $(Li^+)_n$ CIP and AGG formation. The Raman spectrum for the C-O-C stretching from Me_2O is shown in **Fig. 2e**. The characteristic peak of pure Me_2O, centered at 917.3 cm^{-1}, shifts slightly to 915.6 cm^{-1} in the Sat. LiFSI-Me_2O electrolyte. Simultaneously, peak broadening is observed, indicating enhanced interactions within the $Li^+(Me_2O)_x(FSI^-)_y$ clusters as the LiFSI salt concentration increases. This redshift is a distinctive feature of weakly solvating monodentate

10.1002/anie.202420411

ethers, where increasing Li^+-Me_2O-FSI^- coordination leads to a shift toward lower wavenumbers. This observation is further corroborated by the molecular dynamics (MD) results discussed in a later section. As shown in **Fig. 2f**, the behavior of bidentate DME contrasts with that of monodentate Me_2O. DME exhibits strong chelation with Li^+, as evidenced by the disappearance of free DME peaks at higher salt concentrations, transitioning from 1 M to more concentrated solutions. This phenomenon aligns with findings from existing literature[29]. To further compare the solvation power of DME and Me_2O, we conducted ^7Li NMR spectroscopy on different electrolytes (**Fig. 2g**). The results reveal that Sat. LiFSI-Me_2O exhibits a broader peak with a downfield (more positive) shift compared to Sat. LiFSI-DME, indicating Me_2O's lower solvation power and the presence of multiple solvation states. These findings also align with the Raman spectrum results (**Fig. 2d and 2e**). In contrast, the NMR spectra for LiFSI in DME are more defined, with shifts that accurately mirror the alterations in Li^+ solvation structure across different LiFSI concentrations. This consistency further highlights DME's strong Li^+-solvent interactions due to its chelating nature, as reported in other studies[30].

10.1002/anie.202420411

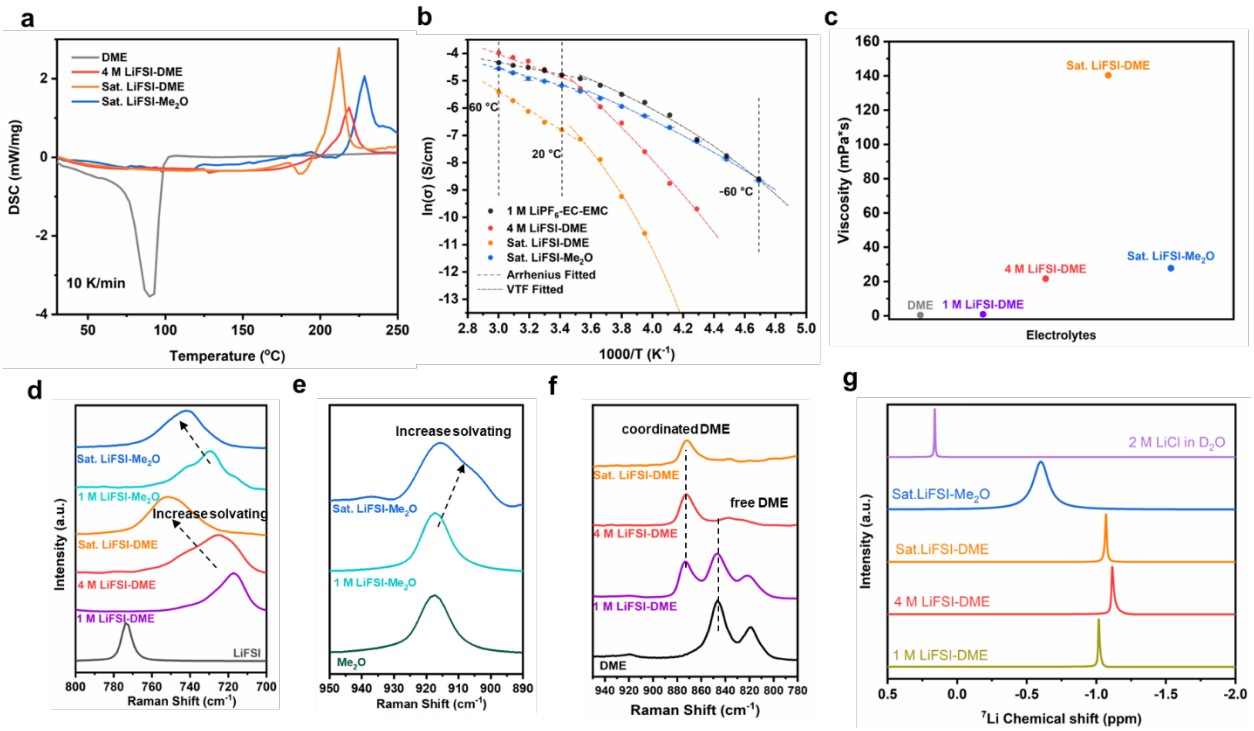

Figure 2. Physical and electrochemical properties of different electrolytes. (a) DSC results (b) Ionic conductivity results; (c) Viscosity measurement; Raman spectra of (d) S-N-S stretching from FSI^-, (e) C-O-C stretching from Me_2O, and (f) C-O-C asymmetric stretching from DME; and (g) NMR spectra.

To elucidate the formation mechanisms of LiFSI-Me_2O complexes, we utilize MD simulations to analyze the DME and Me_2O electrolytes across a range of molecular ratios (**Fig. 3a**). First, we predict the condensation behavior of various Me_2O:LiFSI systems at molar ratios ranging from 20:1 – 2:1, corresponding to a range from dilute salt concentrations to a relatively high salt concentration. These systems are constructed where LiFSI agglomerates are placed in contact with gaseous Me_2O and then investigated at 1 bar of applied pressure as managed by an isothermal-isobaric Noose-Hoover barostat (see computational methods). As shown in **Fig. 3b and Supplementary Fig. 4**, we observe a sharp increase in system density to ~ 1.02 g mL^{-1} within 2 ns for system molar ratios at Me_2O:LiFSI $\leqslant$ 2.3:1, whereas every other system maintains total densities of << 0.1 g mL^{-1}. When examining the trajectories (**Fig. 3a**), this indicates a favorable

condensation for Me_2O:LiFSI 2.3:1 into the liquid phase driven by salt dissolution. The Me_2O:LiFSI 2.3:1 molar ratio aligns well with experimental measurements (**Supplementary Fig. 1 and Supplementary Table 3**), suggesting that the Coulombic condensation phenomena can be accurately predicted in future systems through computational methods. To further investigate the local environment of Li^+ in the Sat. LiFSI-Me_2O relative to the conventional DME-based systems, we conduct radial distribution function (RDF) analysis on the systems of interest over 10 ns (see computational methods). As shown in **Supplementary Fig. 5a** and **5b**, the probability of Li^+/Me_2O coordination is significantly reduced compared to Li^+/DME coordination. In contrast, the probability of Li^+/FSI^- coordination in saturated LiFSI-Me_2O is comparable to that in saturated LiFSI-DME. Furthermore, in the case of 1 M LiFSI-Me_2O, the Li^+/FSI^- coordination probability aligns closely with that of 4 M LiFSI-DME. Based on the relative number density of coordinating species, we predict average solvation structures of $Li^+(DME)_{3.0}$, $Li^+(DME)_{2.7}$ $(FSI^-)_1$, and $Li^+(DME)_{0.85}$ $(FSI^-)_{3.1}$ for 1 M, 4 M and Sat. LiFSI-DME, respectively (note that 1 DME contains 2 oxygen atoms) (**Supplementary Fig. 5c and 5d**). In Me_2O-based systems, the predicted solvation structures are $Li^+(Me_2O)_{3.2}(FSI^-)_{1.0}$ for 1 M LiFSI-Me_2O and $Li^+(Me_2O)_{0.9}$ $(FSI^-)_{3.7}$ for Sat. LiFSI-Me_2O (**Supplementary Fig. 5c, 5d and 5e**). Such highly aggregated solvation structures are commonly associated with salt-derived SEI chemistries when applied in Li-metal batteries, but are also typically associated with poor transport and elevated solution viscosity as previously discussed[31]. In Sat. LiFSI-Me_2O, however, these negative externalities are substantially mitigated while maintaining such beneficial solvation properties.

10.1002/anie.202420411

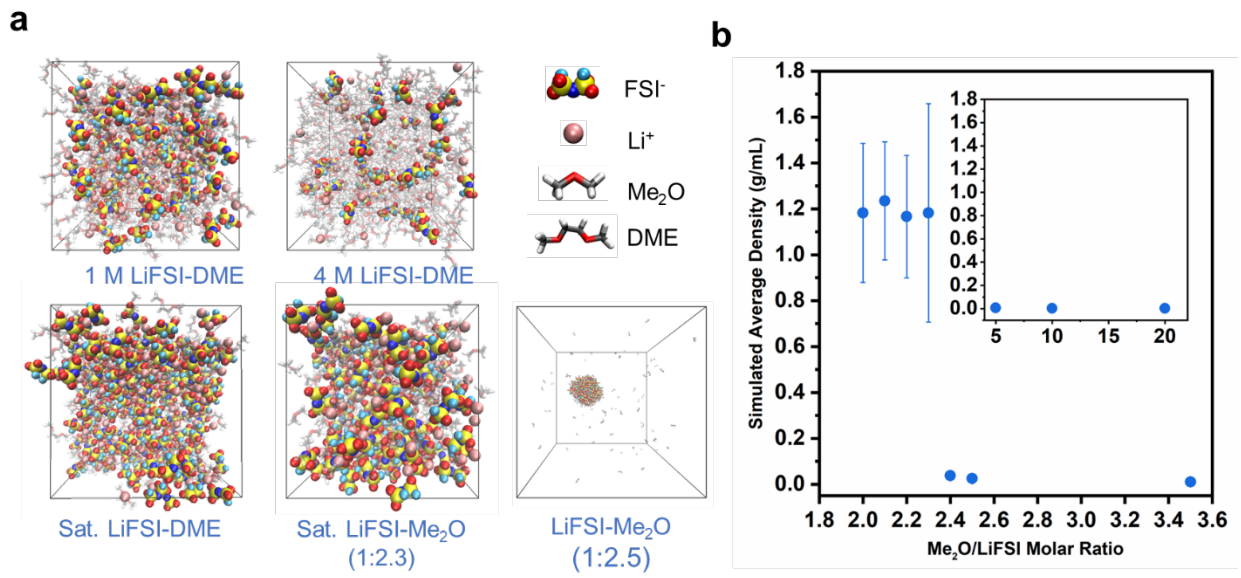

Figure 3. Solvation structure and MD simulation results of the formulated electrolytes. (a) Snapshots of the MD simulation cell containing the representative Li^+ solvates. Colors: Li^+, pink; C, dark grey; O, red; S, yellow; N, naval blue; F, cyan; H, white. (b) Calculated densities for different Me_2O:LiFSI molar ratios.

Leveraging our insights into the properties and molecular dynamics of the LiFSI-Me_2O electrolyte, our next step involves evaluating its compatibility with a Li-metal anode across various temperatures. The stability of Li-metal cycling was investigated by Li/Cu plating and stripping tests. Cells with 4 M LiFSI-DME, Sat. LiFSI-Me_2O, and Sat. LiFSI-DME were tested in Li||Cu configuration at a current density of 0.5 mA cm^{-2}. As depicted in **Fig. 4a**, both 4 M LiFSI-DME and Sat. LiFSI-Me_2O systems show consistent Li-metal anode cycling over 1000 cycles at room temperature. However, Sat. LiFSI-DME system exhibits more significant cycling fluctuations mainly due to its high viscosity with the 4 M LiFSI-DME showing a higher average plating voltage compared to Sat. LiFSI-Me_2O (**Supplementary Fig. 6**). To assess the wide-temperature operability of these electrolytes, Li-half cells utilizing 4 M LiFSI-DME and Sat. LiFSI-Me_2O were cycled at –20℃, –40 ℃, and 50℃. The Sat. LiFSI-Me_2O system maintains CE values of 98.4%, 98.4%, and 99.0% respectively at these temperatures (**Fig. 4b**). In contrast, the 4 M LiFSI-DME

system proved ineffective at lower temperatures, only achieving comparable Li-metal performance to the Sat. LiFSI-Me_2O system at 50 °C, with a CE of 99% (**Fig. 4b**). The reduction in overpotential of Li/Cu cells in the 4 M LiFSI-DME system at higher temperatures can be attributed to enhanced electrolyte transport, but it's worth noting that the electrolyte's ionic conductivity decreases significantly, leading to soft shorting at lower temperatures[32],[33]. Furthermore, we systematically investigated charge toughness by varying the current density from 0.5 mA cm^{-2} to 12 mA cm^{-2}. As depicted in **Supplementary Fig. 7**, cells utilizing Sat. LiFSI-Me_2O demonstrate stable cycling even at a critical current density of 12 mA cm^{-2}. Conversely, cells using Sat. LiFSI-DME experienced shorting at 3 mA cm^{-2}, and the CE for cells utilizing 4 M LiFSI-DME decrease to 95.5% as the applied current reached 3 mA cm^{-2}. This further underscore the resilience of the Sat. LiFSI-Me_2O electrolyte, which can withstand high-current Li-metal cycling.

The deposited Li morphology was characterized from 4 M LiFSI-DME and Sat. LiFSI-Me_2O systems to further understand the Li cycling behaviors. After depositing 3 mAh cm^{-2} at 3 mA cm^{-2} in both electrolytes at room temperature, the cross-section and surface morphology (**Fig. 4c,d,e,f**) of the plated Li at first cycle were analyzed. While both systems exhibit a locally dense surface structure with large lithium chunks, the 4 M LiFSI-DME system shows a greater thickness growth and larger porosity in the deposited Li (**Fig. 4c**). On the contrary, the plated Li in the Sat. LiFSI-Me_2O system (**Fig. 4e**) exhibits fewer voids and an exceptionally dense morphology with a thickness closely matching the theoretical plated capacity (theoretical = 14.85 μm). This explains the deposited Li morphology as a pivotal point to achieve high CE cycling.

10.1002/anie.202420411

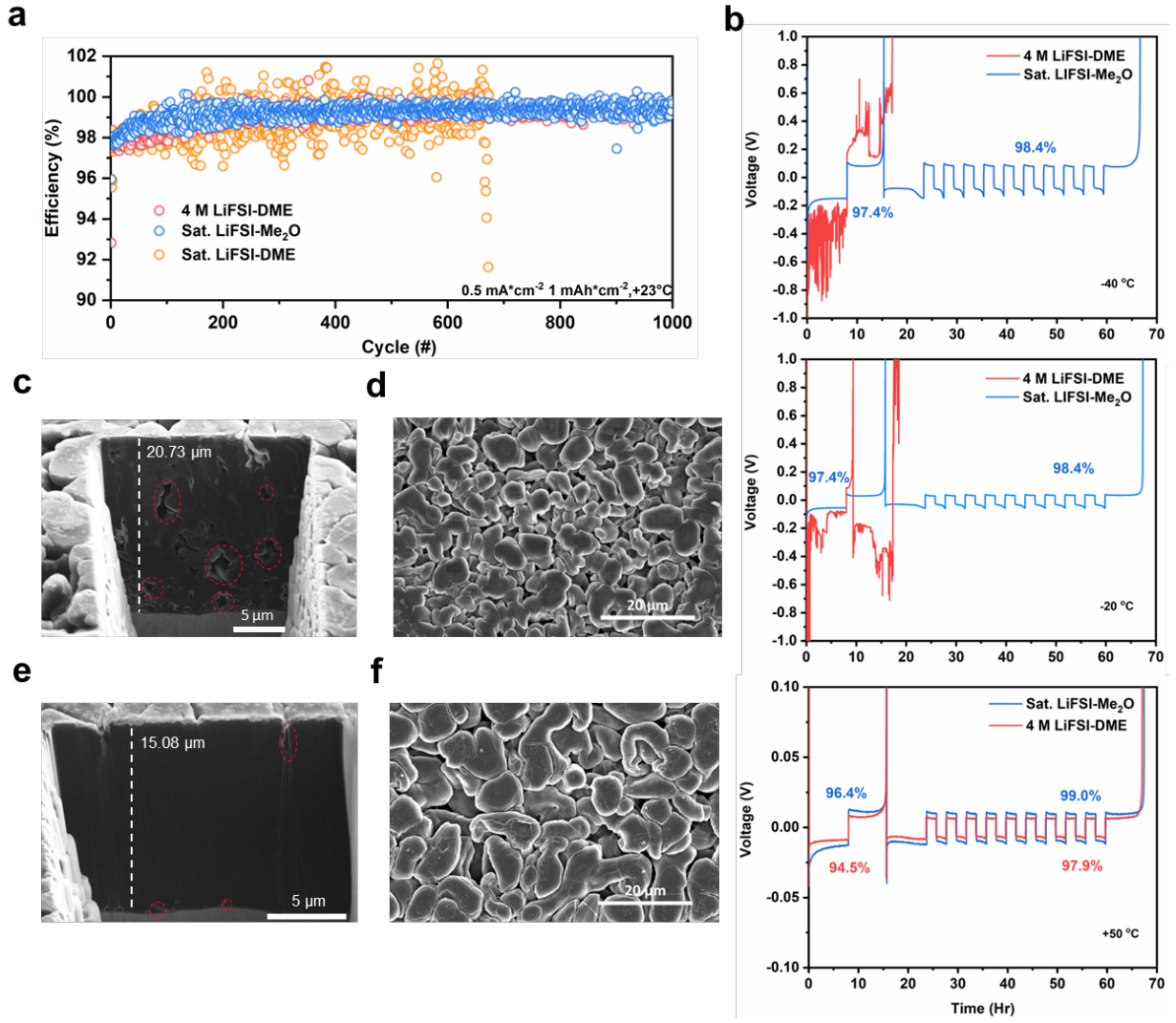

Figure 4. Electrochemical cycling evaluations of Li/Cu cells. (a,b) Electrochemical performance of Li/Cu plating and stripping at different temperatures. (c,d,e,f) Visualization of deposited Li surface and cross-section morphology in different electrolytes at first cycle electrochemically deposition (c, d: 4 M LiFSI-DME; e, f: Sat. LiFSI-Me_2O).

To evaluate the full-cell performance of the Sat. LiFSI-Me_2O, a SPAN cathode was selected owing to its low-cost, high cycling stability, and good kinetics. Furthermore, with modest voltage window, SPAN should accommodate the limited oxidative stability of typical ether electrolytes[34]. As depicted in **Fig. 5a**, the cell utilizing 4 M LiFSI-DME shows less than 50 cycles when reaching to 80% capacity retention, while the cell with Sat. LiFSI-Me_2O maintains over 85%

capacity retention even after 200 cycles. This improved performance is attributed to the lower voltage polarization observed between the average charge and discharge voltages in the Sat. LiFSI-Me_2O cell (**Supplementary Fig. 8**). In contrast, the Sat. LiFSI-DME system exhibits minimal initial capacity during C/10 cycling due to the high viscosity of the electrolyte (**Supplementary Fig. 9**). To further investigate the temperature resilience of the electrolytes, cells were cycled at -20 °C and +50 °C. At -20 °C, the Sat. LiFSI-Me_2O electrolyte enabled Li/SPAN cells to retain 280 mAh g^{-1} after 60 cycles, while the cell using 4 M LiFSI-DME exhibited almost no discharge capacity (**Fig. 5b**), likely due to high cell impedance from sluggish electrolyte transport, consistent with observations from Li/Cu cycling. At -40 °C, the Sat. LiFSI-Me_2O electrolyte can still maintain 50% of the room temperature discharge capacity when charging and discharging (**Supplementary Fig. 10**). At 50 °C, cells with Sat. LiFSI-Me_2O and 4 M LiFSI-DME retained 97% and 46% capacity after 50 cycles, respectively (**Fig. 5c**). This stark contrast is attributed to the significant increase in cell impedance in the 4 M LiFSI-DME system at elevated temperatures (**Supplementary Fig. 11**). Moreover, the fast-charging evaluation of the Li||SPAN full-cell is conducted with a limited 50 μm Li-metal anode. As for the cell cycled in 4 M LiFSI-DME, it demonstrates severe capacity fade after 30 cycles, while the Sat. LiFSI-Me_2O system manages to deliver consistent cycling performance across 100 cycles (**Fig. 5d**). To investigate the underlying cause of impedance growth at both room and elevated temperatures, we hypothesize that the lithium polysulfide shuttle effect may play a key role. To qualitatively assess this, 0.25 M Li_2S_6 was soaked in both electrolytes for one day to visually observe color changes. As shown in **Fig. 5e**, the Sat. LiFSI-Me_2O electrolyte displayed minimal polysulfide dissolution compared to 4 M LiFSI-DME, likely due to the weaker coordination between Li^+ and Me_2O, which reduces the dissociation of the Li-S ionic bond. In contrast, DME is known for its strong cleaving effect on

10.1002/anie.202420411

Li^+, leading to higher Li_xS_y solubility in 4 M LiFSI-DME[35]. These results indicate that Sat. LiFSI-Me_2O outperforms 4 M LiFSI-DME in Li/SPAN systems across multiple performance metrics (**Fig. 5f**).

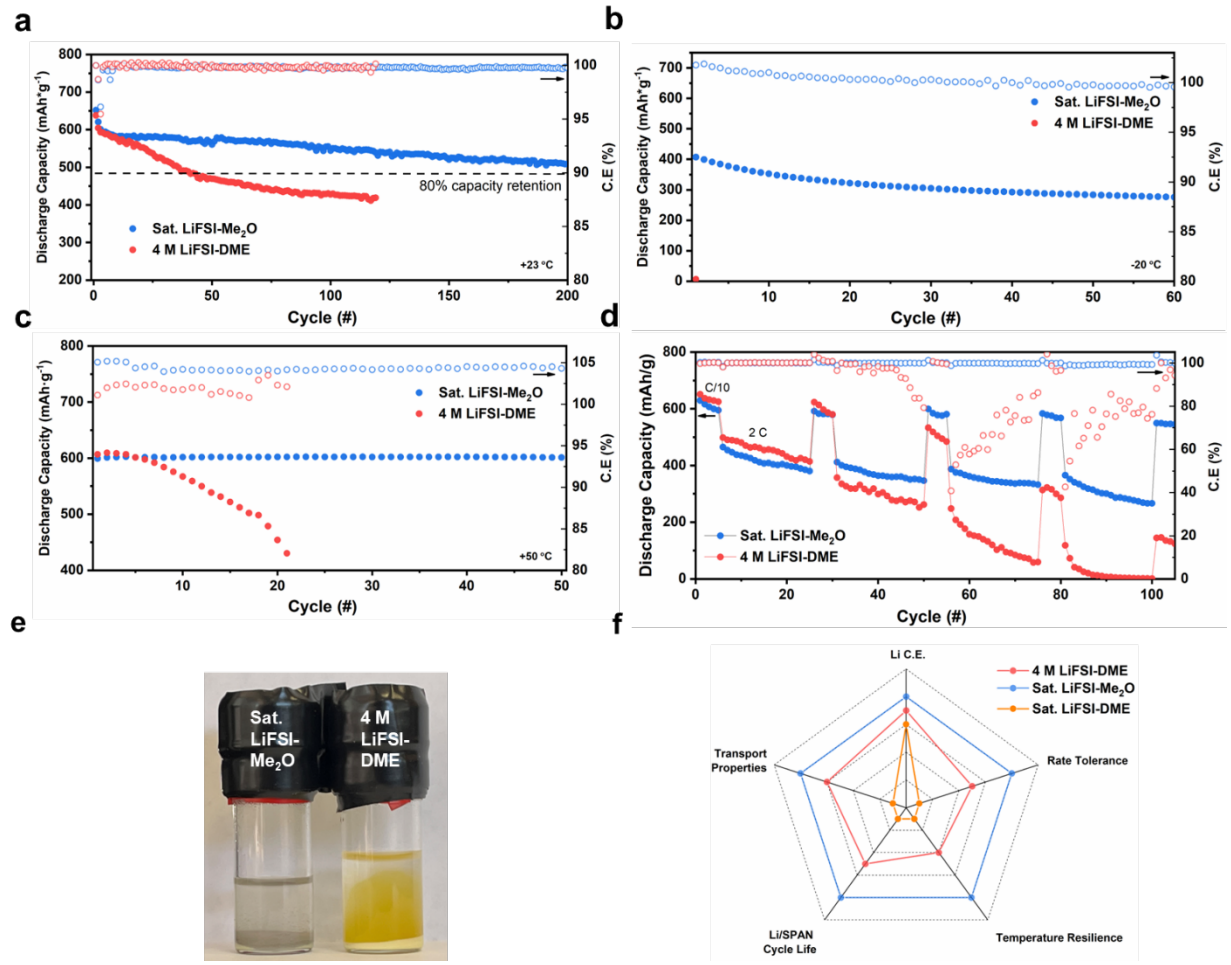

Figure 5. Electrochemical cycling evaluations of Li/SPAN cells with different electrolytes and 3.2 mAh cm^{-2} SPAN areal loading. (a) Long-term electrochemical cycling of 250 um Li-metal in Li/SPAN cells at room temperature (b) Electrochemical cycling of Li/SPAN cells at -20 °C. (c) Electrochemical cycling of Li/SPAN cells at 50 °C. (d) Fast charging evaluations of 50 µm Li-metal in Li/SPAN cells, the applied current is C/10 for every 5 cycles followed by 2C for every 20 cycles. (e) The optical images of polysulfide Li_xS_y soaked in different electrolytes after one day at room temperature. (f) Radar chart of performance metrics of studied electrolytes.

The chemical compositions of the CEI and SEI on cycled Li metal and SPAN electrodes within Li/SPAN cells were characterized through X-Ray Photoelectron Spectroscopy (XPS) to

10.1002/anie.202420411

elucidate the impact of the electrolyte on interfacial chemistry. As shown in **Fig. 6a and 6b**, a higher concentration of Li_2S is observed in the S 2p spectra on the Li-metal cycled in the 4 M LiFSI-DME system, while a lower amount is found in the Sat. LiFSI-Me_2O system. Similarly, from the de-lithiated SPAN samples (**Fig. 6c and 6d**), we observe a similar trend, with SPAN cycled in the 4 M LiFSI-DME system generating a higher Li_2S compositional ratio compared to its counterpart in the Sat. LiFSI-Me_2O system. This disparity can be attributed to the dissolved polysulfides shuttling from SPAN to the Li-metal, facilitated by the higher solubility in the 4 M LiFSI-DME system. However, little difference is observed in the O 1s, F 1s spectra, and the overall Li atomic ratio, indicating their similarity in terms of the LiF-dominated SEI chemistry coupled with carbonyl compounds, Li_xSO_y, and Li_2O (**Supplementary Fig. 12 and 13**). To isolate the sulfur signal on the cycled Li as a result of polysulfide shuttling from the SPAN electrode, we conducted a parallel experiment involving XPS analysis on deposited Li in Li/Cu (**Supplementary Fig. 14 and 15**). As depicted in **Supplementary Fig. 115**, a higher amount of Li_2S is observed on the cycled Li when using the Sat. LiFSI-Me_2O electrolyte, indicating a greater degree of salt decomposition compared to cycled Li using the 4 M LiFSI-DME electrolyte. This finding provides additional evidence that the improved performance of the Li/SPAN system is attributed to reduced polysulfide dissolution and the presence of a salt-derived SEI containing LiF, Li_2O, Li_2S and Li_xSO_y.

10.1002/anie.202420411

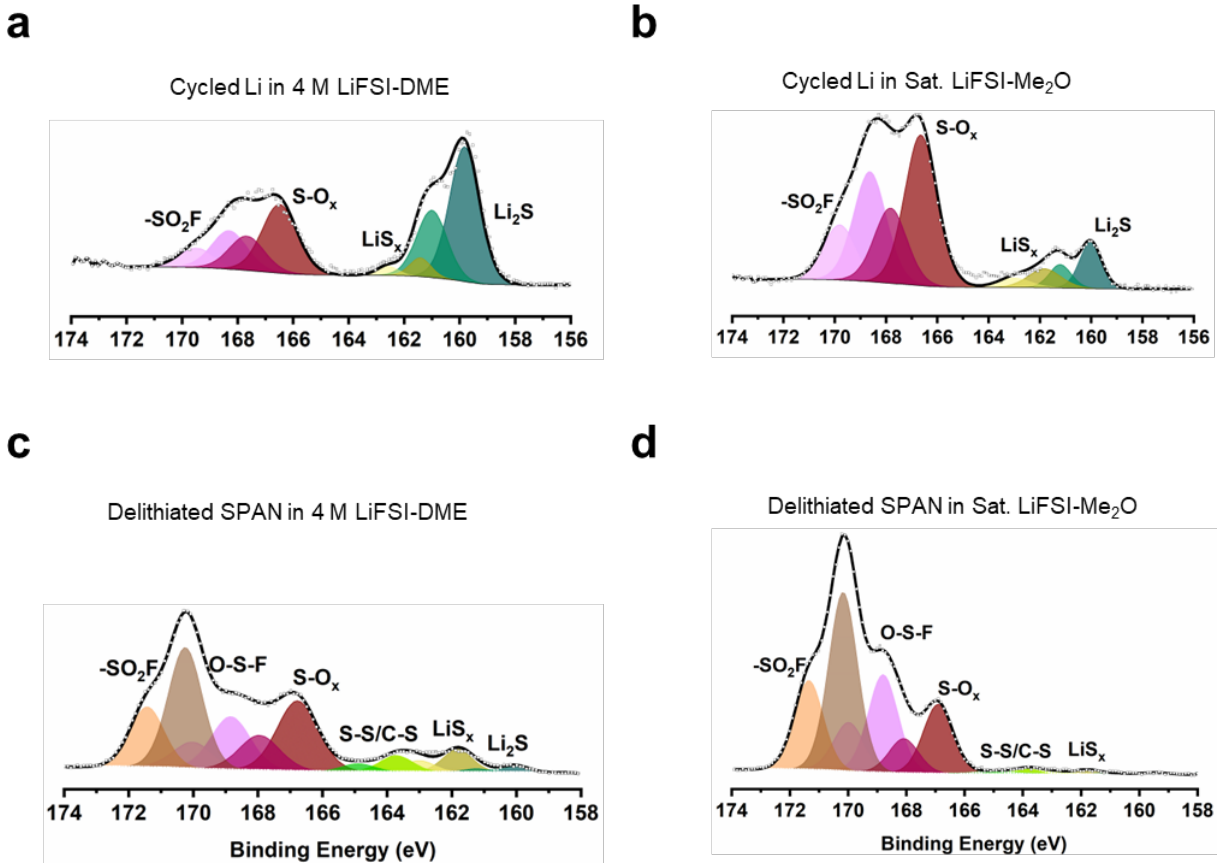

Figure 6. Interface analysis of the cycled Li and SPAN from the fully charged Li/SPAN cells at 60th cycle. (a-d) Local XPS S 2p spectra of cycled Li and delithiated SPAN in the 4 M LiFSI-DME electrolyte (a,c) and the Sat. LiFSI-Me_2O electrolyte (b,d).

Conclusion

Me_2O gas was demonstrated to be condensed into liquid phase at ambient conditions by employing a high LiFSI salt concentration to facilitate Coulombic condensation (Li^+-Me_2O ion-dipole interaction). Such electrolyte exhibits anion-pair solvation structures and moderate ionic conductivities over a wide-temperature range. By formulating a saturated LiFSI-Me_2O electrolyte, we achieved excellent cyclability of lithium metal over 1000 cycles and the ability to withstand critical current densities up to 12 mA cm^{-2}. When combined with a SPAN electrode, the saturated

LiFSI-Me_2O electrolyte demonstrated superior performance compared to a 4 M LiFSI-DME electrolyte. This improvement can be attributed to the formation of a salt-derived solid electrolyte interphase at the lithium metal anode and reduced dissolution of polysulfides, as verified by XPS and polysulfide soak tests. Despite these advantages, further optimization of Sat. LiFSI-Me_2O is needed to address challenges under conditions closer to practical applications, such as lean electrolyte configurations and limited lithium reservoirs. These refinements are essential for achieving long-term stability and ensuring the electrolyte's applicability in commercial battery systems. The study provides a new design strategy for high concentration electrolytes with low viscosity and low polysulfide solubilities for Li/sulfur systems. It also offers a potential strategy to design recyclable electrolytes and battery systems by manipulating solvent-salt interactions.

Acknowledgements:

This work was supported partially by an Early Career Faculty grant from NASA's Space Technology Research Grants Program (ECF 80NSSC18K1512) to Z.C. This material is partially based upon work supported by the U.S. Department of Energy's Office of Energy Efficiency and Renewable Energy (EERE) under the Vehicles Technology Office Award Number DE-0010399 (Z. C.). Y. Y. acknowledged the dissertation year fellowship from Materials Science Program at UC San Diego. The SEM were performed in part at the San Diego Nanotechnology Infrastructure (SDNI) of UC San Diego, a member of the National Nanotechnology Coordinated Infrastructure, which was supported by the National Science Foundation (Grant ECCS-1542148).Y. Y. thanks Ich C. Tran for their help regarding XPS experiments performed at the University of California Irvine Materials Research Institute (IMRI) using instrumentation funded in part by the National Science Foundation Major Research Instrumentation Program (grant CHE-1338173). The authors acknowledge the use of Raman instrumentation supported by NSF through the UC San Diego Materials Research Science and Engineering Center (UCSD MRSEC), grant # DMR-2011924. Y. Y. acknowledged the discussion of NMR results with Dr. Zhiao Yu from Stanford University and Dr. Xianggeng Liu from University of Massachusetts, Amherst.

Author Contributions:

Y.Y., J.H., Y.S.M., and Z.C. conceived the original idea. Y.Y., J.H., and Z.C. designed the experiments. Y.Y., J.H., and K.K. carried out the experiments. J. H. developed force field and conducted the MD simulations. B.B. performed the TGA and DSC. K.Y., A.L., M.L., and G.R. assisted with control experiments. B.L. performed the FIB-SEM characterization. Y.Y and W.L. performed the XPS characterization and analysis. H.P conducted NMR analysis. Y.Y, J.H., and A.L. prepared the manuscript with input from all co-authors. S.W. provided insightful suggestions to the manuscript. All authors have given approval to the final version of the manuscript.

Declaration of Interests:

No potential competing interest was reported by the authors.

Keywords: Li/Sulfur Batteries; Electrolyte; Solvation structure; Ion-dipole interaction; Fast Charge

References

[1] G. M. Hobold, J. Lopez, R. Guo, N. Minafra, A. Banerjee, Y. Shirley Meng, Y. Shao-Horn, B. M. Gallant, *Nature Energy* **2021**, *6*, 951-960.
[2] C. Fang, J. Li, M. Zhang, Y. Zhang, F. Yang, J. Z. Lee, M.-H. Lee, J. Alvarado, M. A. Schroeder, Y. Yang, *Nature* **2019**, *572*, 511-515.
[3] J. Wang, J. Yang, C. Wan, K. Du, J. Xie, N. Xu, *Advanced Functional Materials* **2003**, *13*, 487-492.
[4] S. Wei, L. Ma, K. E. Hendrickson, Z. Tu, L. A. Archer, *Journal of the American Chemical Society* **2015**, *137*, 12143-12152.
[5] S. Wang, B. Lu, D. Cheng, Z. Wu, S. Feng, M. Zhang, W. Li, Q. Miao, M. Patel, J. Feng, *Journal of the American Chemical Society* **2023**, *145*, 9624-9633.
[6] H. Liu, J. Holoubek, H. Zhou, A. Chen, N. Chang, Z. Wu, S. Yu, Q. Yan, X. Xing, Y. Li, *Materials Today* **2021**, *42*, 17-28.
[7] Z. Wu, H. Liu, J. Holoubek, C. Anderson, L. Shi, H. Khemchandani, D. Lu, D. Liu, C. Niu, J. Xiao, *ACS Energy Letters* **2022**, *7*, 2701-2710.
[8] J. Lei, J. Chen, A. Naveed, H. Zhang, J. Yang, Y. Nuli, J. Wang, *ACS Applied Energy Materials* **2021**, *4*, 5706-5712.
[9] D. Aurbach, E. Pollak, R. Elazari, G. Salitra, C. S. Kelley, J. Affinito, *Journal of The Electrochemical Society* **2009**, *156*, A694.

[10] S. S. Zhang, *Electrochimica Acta* **2012**, *70*, 344-348.
[11] J. Holoubek, H. Liu, Z. Wu, Y. Yin, X. Xing, G. Cai, S. Yu, H. Zhou, T. A. Pascal, Z. Chen, *Nature energy* **2021**, *6*, 303-313.
[12] G. Cai, J. Holoubek, M. Li, H. Gao, Y. Yin, S. Yu, H. Liu, T. A. Pascal, P. Liu, Z. Chen, *Proceedings of the National Academy of Sciences* **2022**, *119*, e2200392119.
[13] J. Qian, W. A. Henderson, W. Xu, P. Bhattacharya, M. Engelhard, O. Borodin, J.-G. Zhang, *Nature communications* **2015**, *6*, 6362.
[14] P. Bai, J. Li, F. R. Brushett, M. Z. Bazant, *Energy & Environmental Science* **2016**, *9*, 3221-3229.
[15] J. Zheng, G. Ji, X. Fan, J. Chen, Q. Li, H. Wang, Y. Yang, K. C. DeMella, S. R. Raghavan, C. Wang, *Advanced Energy Materials* **2019**, *9*, 1803774.
[16] S. Chen, J. Zheng, D. Mei, K. S. Han, M. H. Engelhard, W. Zhao, W. Xu, J. Liu, J. G. Zhang, *Advanced materials* **2018**, *30*, 1706102.
[17] X. Cao, P. Gao, X. Ren, L. Zou, M. H. Engelhard, B. E. Matthews, J. Hu, C. Niu, D. Liu, B. W. Arey, C. Wang, J. Xiao, J. Liu, W. Xu, J.-G. Zhang, *Proceedings of the National Academy of Sciences* **2021**, *118*, e2020357118.
[18] C.-C. Su, M. He, R. Amine, T. Rojas, L. Cheng, A. T. Ngo, K. Amine, *Energy & Environmental Science* **2019**, *12*, 1249-1254.
[19] C. M. Efaw, Q. Wu, N. Gao, Y. Zhang, H. Zhu, K. Gering, M. F. Hurley, H. Xiong, E. Hu, X. Cao, W. Xu, J.-G. Zhang, E. J. Dufek, J. Xiao, X.-Q. Yang, J. Liu, Y. Qi, B. Li, *Nature Materials* **2023**, *22*, 1531-1539.
[20] X. Cao, H. Jia, W. Xu, J.-G. Zhang, *Journal of The Electrochemical Society* **2021**, *168*, 010522.
[21] Y. Yin, Y. Yang, D. Cheng, M. Mayer, J. Holoubek, W. Li, G. Raghavendran, A. Y. Liu, 2022 #9}, B. Lu, D. M. Davies, *Nature Energy* **2022**, *7*, 548-559.
[22] Y. Yin, J. Holoubek, A. Liu, B. Sayahpour, G. Raghavendran, G. Cai, B. Han, M. Mayer, N. B. Schorr, T. N. Lambert, *Advanced Materials* **2023**, *35*, 2207932.
[23] X. Fan, L. Chen, X. Ji, T. Deng, S. Hou, J. Chen, J. Zheng, F. Wang, J. Jiang, K. Xu, *Chem* **2018**, *4*, 174-185.
[24] H. Wang, Z. Yu, X. Kong, S. C. Kim, D. T. Boyle, J. Qin, Z. Bao, Y. Cui, *Joule* **2022**.
[25] Z. Yu, H. Wang, X. Kong, W. Huang, Y. Tsao, D. G. Mackanic, K. Wang, X. Wang, W. Huang, S. Choudhury, *Nature Energy* **2020**, *5*, 526-533.
[26] B. Lu, D. Cheng, B. Sreenarayanan, W. Li, B. Bhamwala, W. Bao, Y. S. Meng, *ACS Energy Letters* **2023**, *8*, 3230-3238.
[27] P. Zheng, X. Meng, J. Wu, Z. Liu, *International Journal of Thermophysics* **2008**, *29*, 1244-1256.
[28] J. Holoubek, K. Kim, Y. Yin, Z. Wu, H. Liu, M. Li, A. Chen, H. Gao, G. Cai, T. A. Pascal, *Energy & Environmental Science* **2022**, *15*, 1647-1658.
[29] Y. Chen, Z. Yu, P. Rudnicki, H. Gong, Z. Huang, S. C. Kim, J.-C. Lai, X. Kong, J. Qin, Y. Cui, *Journal of the American Chemical Society* **2021**, *143*, 18703-18713.
[30] Y. Chen, S.-L. Liao, H. Gong, Z. Zhang, Z. Huang, S. C. Kim, E. Zhang, H. Lyu, W. Yu, Y. Lin, *Chemical Science* **2024**.
[31] L. Suo, Y.-S. Hu, H. Li, M. Armand, L. Chen, *Nature communications* **2013**, *4*, 1481.
[32] Y. Gao, T. Rojas, K. Wang, S. Liu, D. Wang, T. Chen, H. Wang, A. T. Ngo, D. Wang, *Nature Energy* **2020**, *5*, 534-542.
[33] Y. Yang, D. M. Davies, Y. Yin, O. Borodin, J. Z. Lee, C. Fang, M. Olguin, Y. Zhang, E. S. Sablina, X. Wang, *Joule* **2019**, *3*, 1986-2000.
[34] A. L. Phan, P. M. Le, C. Wang, *Joule* **2024**.
[35] A. Gupta, A. Bhargav, A. Manthiram, *Advanced energy materials* **2019**, *9*, 1803096.
[36] Z. Wu, S.-M. Bak, Z. Shadike, S. Yu, E. Hu, X. Xing, Y. Du, X.-Q. Yang, H. Liu, P. Liu, *ACS Applied Materials & Interfaces* **2021**, *13*, 31733-31740.
[37] D. M. Davies, Y. Yang, E. S. Sablina, Y. Yin, M. Mayer, Y. Zhang, M. Olguin, J. Z. Lee, B. Lu, D. Damien, *Journal of Power Sources* **2021**, *493*, 229668.

[38] A. S. Gouveia, C. E. Bernardes, L. C. Tomé, E. I. Lozinskaya, Y. S. Vygodskii, A. S. Shaplov, J. N. C. Lopes, I. M. Marrucho, *Physical Chemistry Chemical Physics* **2017**, *19*, 29617-29624.

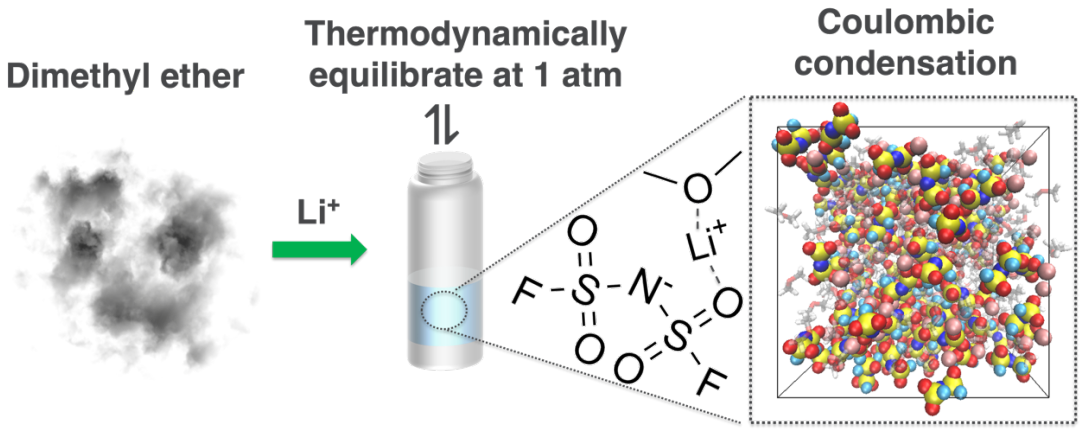

Graphical abstract:

Dimethyl ether (Me_2O) gas can be condensed through ion-dipole interactions with lithium bis(fluorosulfonyl)imide at sufficiently high concentrations, which elevates the boiling of point Me_2O, imparting enhanced physical and electrochemical properties for battery applications. The approach of Coulombic condensation by facilitating ion-dipole interactions with weakly coordinating solvents offers a promising strategy for next-generation electrolyte design.